The Murmur of The Hidden Monster: *Chandra*'s Decadal View of The Super-massive Black Hole in M31

Zhiyuan Li[1], Michael R. Garcia[1], William R. Forman[1], Christine Jones[1], Ralph P. Kraft[1], Dharam V. Lal[1], Stephen S. Murray[1,2], Q. Daniel Wang[3]

ABSTRACT

The Andromeda galaxy (M31) hosts a central super-massive black hole (SMBH), known as M31*, which is remarkable for its mass ($\sim 10^8$ M$_\odot$) and extreme radiative quiescence. Over the past decade, the *Chandra X-ray observatory* has pointed to the center of M31 $\sim$100 times and accumulated a total exposure of $\sim$900 ks. Based on these observations, we present an X-ray study of a highly variable source that we associate with M31* based on positional coincidence. We find that M31* remained in a quiescent state from late 1999 to 2005, exhibiting an average 0.5-8 keV luminosity $\lesssim 10^{36}$ ergs s^{-1}, or only $\sim 10^{-10}$ of its Eddington luminosity. We report the discovery of an outburst that occurred on January 6, 2006, during which M31* radiated at $\sim 4.3 \times 10^{37}$ ergs s^{-1}. After the outburst, M31* entered a more active state that apparently lasts to the present, which is characterized by frequent flux variability around an average luminosity of $\sim 4.8 \times 10^{36}$ ergs s^{-1}. These flux variations are similar to the X-ray flares found in the SMBH of our Galaxy (Sgr A*), making M31* the second SMBH known to exhibit recurrent flares. Future coordinated X-ray/radio observations will provide useful constraints on the physical origin of the flaring emission and help rule out a possible stellar origin of the X-ray source.

Subject headings: galaxies: individual (M31) – galaxies: nuclei – X-rays: galaxies

1. Introduction

Most, if not all, galaxies with a stellar bulge are thought to harbor a super-massive black hole (SMBH) in their nuclei. Accretion onto and feedback (i.e., both radiative and

[1]Harvard-Smithsonian Center for Astrophysics, 60 Garden Street, Cambridge, MA 02138; zyli@cfa.harvard.edu

[2]Johns Hopkins University, 3400 North Charles St., Baltimore, MD 21205

[3]Department of Astronomy, University of Massachusetts, 710 North Pleasant Street, Amherst, MA 01003

mechanical energy output) from the SMBH is one of the fundamental astrophysical processes that govern galaxy evolution. Compared to their high-redshift counterparts, most SMBHs in the local universe, when observed, are found to be radiatively quiescent (e.g., Zhang et al. 2009; Gallo et al. 2010), and are often dubbed low-luminosity active galactic nuclei (LLAGNs; cf. Ho 2008). By analogy to Galactic black hole binaries in a low/hard state (cf. McClintock & Remillard 2006), LLAGNs are generally thought to be powered by radiatively inefficient, advection-dominated accretion and/or outflow (Narayan & Yi 1994; Blandford & Begelman; Quataert & Gruzinov 2000) that operate at very sub-Eddington accretion rates[1]. Albeit often subject to instrumental limitations as a consequence of their radiative quiescence, studies of LLAGNs have important implications for accretion physics, fueling and feedback mechanisms, and black hole growth over cosmic time.

A well-known LLAGN is the SMBH in our Galaxy, Sgr A* (cf. Melia & Falcke 2001), which has an extremely quiescent bolometric luminosity of $\sim 3 \times 10^{-9} L_{\mathrm{Edd}}$ (for its mass of $\sim 4 \times 10^6$ M$_\odot$; Ghez et al. 2003), a factor of $10^2 - 10^6$ lower than the inferred values for most LLAGNs (e.g., Zhang et al. 2009; Ho 2009). More unusual about Sgr A* is its flaring emission detected in X-ray, infrared and radio bands (Baganoff et al. 2001; Genzel et al. 2003; Zhao et al. 2003). In particular, the X-ray flares show the greatest variability, with hour-timescales and peak fluxes reaching $\sim$10-100 times the quiescent level (e.g., Baganoff et al. 2001; Porquet et al. 2003, 2008). In contrast, most LLAGNs show only a modest level of X-ray variability (e.g., Ptak et al. 1998).

Until now, Sgr A* has remained the only LLAGN found to exhibit recurrent flares. In this *Letter*, we report the discovery of flaring X-ray emission from the SMBH in M31, based on the most up-to-date data obtained from the *Chandra X-ray Observatory* (Weisskopf et al. 2002). A distance of 780 kpc is adopted for M31. We quote 1σ uncertainties throughout this work.

2.   The SMBH in M31

We begin with a brief overview of the most relevant observational aspects of the SMBH in M31. The center of M31 exhibits the well known double-peaked feature in the optical and near-UV (the so-called double nuclei, P1 and P2; Lauer et al. 1993), which is interpreted as an eccentric disk of primarily old stars orbiting around the SMBH (Tremaine 1995). The

---

[1]less than a few percent of the Eddington mass accretion rate $\dot{M}_{\mathrm{Edd}} \equiv 10 L_{\mathrm{Edd}}/c^2$, where $L_{\mathrm{Edd}} = 1.3 \times 10^{38}(M_{\mathrm{BH}}/M_\odot)$ erg s^{-1} is the Eddington luminosity

latter is embedded in P2[2], with an inferred dynamical mass of $1.4^{+0.9}_{-0.3} \times 10^8$ M$_\odot$ (Bender et al. 2005).

Possible counterpart of the SMBH has been detected only in the radio and X-ray bands to date. Using Very Large Array (VLA) observations at 8.4 GHz, Crane, Dickel & Cowan (1992) found an unresolved source, named M31* following the convention of Sgr A*, at a position coincident with P2. A marginal 8.4 GHz flux variation was reported by Crane et al. (1993). Based on a *Chandra*/HRC observation, Garcia et al. (2005) claimed a 2.5 σ detection of X-ray emission from the position of P2. Based on a set of *Chandra*/ACIS observations taken before 2006, Li, Wang & Wakker (2009) determined an intrinsic luminosity of $\sim 1.2 \times 10^{36}$ ergs s^{-1} at the position of P2, which places a firm upper limit to the (quiescent) X-ray emission from the SMBH, corresponding to only $\sim 10^{-10} L_{\rm Edd}$. With more recent *Chandra*/HRC observations, Garcia et al. (2010) reported X-ray flux variations of P2 by a factor of $\sim$3 on a timescale of days and a factor of $\gtrsim$10 in a year. They also detected M31* at 5 GHz with VLA, finding no significant flux variation among four observations near the end of 2004.

3.   Data preparation

In this work, we utilized 98 *Chandra* observations taken between October 13, 1999 and March 5, 2010, which irregularly sampled the time domain. Typically, in each year there were $\sim$10 observations, with two successive observations separated by hours to months. The full dataset consists of 58 ACIS observations and 40 HRC observations. The HRC best employs the angular resolution of the *Chandra* High Resolution Mirror Assembly (HRMA), but essentially lacks spectral resolution. The ACIS has higher broad-band effective area than the HRC, but slightly undersamples the point-spread function (PSF) of the HRMA. The majority of the ACIS observations have exposures of $\sim$5 ks and the aimpoint on the I3 CCD. The HRC observations, all taken with the I-array, have more diverse exposures ranging from 1 to 50 ks. In all cases, the nucleus of M31 was placed within 1$'$ of the aimpoint, and hence was observed with optimal angular resolution.

We reprocessed the data using CIAO version 4.2 and the corresponding calibration files. We followed the standard procedure of data reduction, except that we turned off the sub-pixel position randomization for the ACIS events. To maximize the temporal coverage, we performed no filtering on time intervals of high particle background. We verified that, in all

---

[2]P2 is referred to as the peak that is fainter in the optical but brighter in the near-UV. The UV-peak is further designated as P3 according to Bender et al. (2005)

observations, the instrumental background is negligible compared to the emission from the central few arcseconds of M31. The total ACIS and HRC exposures are 305 ks and 571 ks, respectively. We considered only ACIS events in the 0.5-8 keV range and HRC events in the *PI* range of 10-350, effectively excluding the majority of instrumental events.

A crucial step for our study is to calibrate the relative astrometry among individual observations, which was done by matching the centroids of about 30 discrete, relatively bright sources located within $1'$ (but outside $5''$) of the nucleus. The resulting accuracy is typically better than $0''.1$. For each observation, we also generated an exposure map, primarily to account for the gradual change in the detector effective area. An absorbed power-law spectrum, with a photon-index of 1.7 and an absorption column density $N_{\rm H} = 10^{21}$ cm^{-2}, was adopted to calculate spectral weights when producing the exposure maps. The energy-dependent difference of the effective area between the ACIS-I, ACIS-S3 and HRC-I, was taken into account, assuming the above incident spectrum, so that the quoted count rates throughout this work refer to ACIS-I.

4. Analysis and results

4.1. X-ray sources in the nuclear region of M31

It is known that several bright X-ray sources are present in the nuclear region of M31, challenging a clean isolation of the emission from M31* (Garcia et al. 2000; Li et al. 2009). We first examine the HRC observations, since they have the better angular resolution (PSF FWHM $\approx 0''.4$). Fig. 1a and Fig. 1b show an image of the nuclear region, stacking all HRC observations on the original pixel scale of $0''.1318$. Four X-ray sources are immediately identified within $4''$ of the nucleus. Following Garcia et al. (2005) and Li et al. (2009), we label these sources in Fig. 1a as: P2 for the source positionally coincident with the nucleus, N1 for the source just $\sim 0''.5$ northeast of P2, SSS for the source $\sim 1''.5$ south of N1, and S1 for the source $\sim 2''$ farther south. The positional coincidence between P2 and the nucleus is demonstrated in Fig. 1b, in which *HST*/ACS intensity contours of the optical double-nuclei of M31 (Lauer et al. 1993) are shown. We have registered the HRC and *HST*/ACS images by matching common extra-nuclear sources, resulting in an uncertainty of $\sim 0''.2$ (Garcia et al. 2010). The other three sources are most likely stellar objects (Kong et al. 2002; Di Stefano et al. 2004; Li et al. 2009).

Visual inspection of individual HRC observations reveals that all four sources show some degree of flux variation, with P2 varying most significantly. This can be illustrated by dividing the HRC data into two subsets, the first half consisting of observations taken before

2006 (Fig. 1c; a total exposure of 256 ks) and the second half consisting of observations taken since 2006 (Fig. 1d; a total exposure of 315 ks). Using the three extra-nuclear sources as a reference, it is obvious that P2 has become significantly brighter since 2006. We note that two more sources can be identified in Fig. 1. The fainter one only appears before 2006, located immediately east of SSS; the brighter one only appears since 2006, located at the upper right (northwest) corner of the images. Neither of these two transient sources affects the following analysis and hence will not be discussed further.

We now turn to the ACIS observations. An image stacking all 58 ACIS observations is shown in Fig. 2a, on a pixel scale of $0\rlap{.}''123$ (i.e., one fourth of the original ACIS pixel size) to take advantage of the sub-pixel positioning information that results from telescope dithering and to approximately match the HRC pixel scale. With a PSF FWHM of $\sim 0\rlap{.}''6$, the four sources are again clearly identified. Visual inspection of individual ACIS observations consistently reveals the flux variability in P2. Most dramatically, in an observation taken on January 6, 2006 (ObsID 7136, with an exposure of 5 ks), P2 appears to be by far the brightest source in the field (Fig. 2b), indicating that an outburst has been fortuitously captured. We similarly present two subsets of the ACIS data, i.e, observations taken before 2006 (Fig. 2c; a total exposure of 149 ks) and since 2006 (but excluding ObsID 7136; Fig. 2c; a total exposure of 152 ks). Again, the two subsets show a marked difference in the brightness contrast between P2 and the three extra-nuclear sources.

4.2. A decadal light curve

To obtain a more quantitative view of the flux variability, we construct a light curve for P2. Due to the proximity of the four sources, in particular between N1 and P2, it is crucial to account for the mutual PSF scattering. We adopt a two-dimensional fitting procedure, similar to that employed by Li et al. (2009), to simultaneously determine the fluxes for all four sources in each observation. Specifically, we take the following steps:

(i) From the circumnuclear sources used for calibrating the astrometry (§ 3), we further select relatively isolated ones ($\sim$10), i.e., those without neighboring sources within $4''$. For each observation, we obtain a local PSF image by stacking the selected sources after centroiding. The average PSF for the summed image (be it over a given detector, a given energy range or a given epoch) is then obtained by stacking individual PSF images of the constituent observations.

(ii) With the CIAO tool *Sherpa*, we fit the summed image, using a model consisting of four point-like sources and a constant local background. Each source is represented by a

delta function, whose center and normalization are free parameters. This model is convolved with the average PSF. Only the central $4''$ from the nucleus is considered in the fit (outlined by the circle in Fig. 1a). Given the limited counts in each unbinned pixel, the best-fit is obtained by minimizing the C-statistic (Cash 1979). The fit is robust in determining the source centroids, the chief goal of this step.

(iii) For each observation, we repeat the above fitting procedure, fixing the centroids of all four sources as determined from the summed image. The fit then allows us to determine the flux and its uncertainty, corrected for the local effective exposure, for each source in each observation. Such a procedure not only maximizes the counting statistics, but also properly accounts for the propagation of the dominating error term arising from the mutual PSF scattering.

The resultant decadal light curve of P2 (Fig. 3) shows two prominent features. First, an outburst, preceded by a 6-yr epoch of quiescence, appears on January 6, 2006, during which the flux of P2 reaches a value of $(76.5 \pm 5.9) \times 10^{-3}$ cts s^{-1}. Second, after the outburst, P2 apparently enters a more active state, characterized by frequent flux variations. Summing the observations taken before 2006 and repeating the above fitting procedure, we obtain an average flux of $(0.3 \pm 0.1) \times 10^{-3}$ cts s^{-1}. Similarly, for the observations since 2006 (but excluding ObsID 7136), we find an average flux of $(6.9 \pm 0.3) \times 10^{-3}$ cts s^{-1}. Therefore, the observed flux of the outburst is $\sim$250 times the quiescent level before it, whereas the long-term average flux increases by a factor of $\sim$23 after the outburst. For comparison, the three extra-nuclear sources[3] show a ratio of fluxes since and before 2006 of $\sim$1.1 (N1), $\sim$0.7 (SSS), $\sim$1.5 (S1), respectively, all indicating a nearly constant long-term flux; their maximum-to-mean flux ratios are $\sim$3-5, also suggesting that the flux variation seen in P2 is exceptional.

It is impractical to perform a spectral analysis for P2, due to the limited number of counts in most observations and the contamination of scattered photons from the other sources whose spectral information is also uncertain. Instead, by dividing the ACIS counts into a soft band and a hard band, we estimate the hardness ratio, defined as $HR = (I_{0.5-2~\text{keV}} - I_{2-8~\text{keV}})/(I_{0.5-2~\text{keV}} + I_{2-8~\text{keV}})$, to be -0.11 ± 1.30, -0.76 ± 0.04 and -0.50 ± 0.04 before, during and after the outburst, respectively. While in the first epoch HR is essentially indeterminate, it appears that the emission during the outburst is softer than that in the last epoch. For comparison, a Galactic foreground-absorbed ($N_{\text{H}} = 7 \times 10^{20}$ cm^{-2}) power-law spectrum with a photon-index of 1.8 (2.6) would result in $HR = -0.50(-0.76)$.

---

[3]We will present elsewhere a detailed timing analysis for these three sources as well as other stellar X-ray sources in the M31 bulge.

We thus convert the observed count rates into 0.5-8 keV intrinsic luminosities of 0.2, 43 and 4.8×10^{36} ergs s^{-1} for the three epochs, by assuming a power-law spectrum with a photo-index of 1.8, 2.6 and 1.8, respectively.

We find no statistically significant intra-observation flux variation for the outburst. We note that a typical 5-ks long observation may probe flux variations arising from a region of $\sim 5 \times 10^{-5}$ pc in diameter, roughly 4 times the Schwarzchild radius of the SMBH. Unfortunately, ObsID 7136 is the most isolated observation: no other observation was taken before or after it within several months. Therefore we cannot rule out that P2 stayed at high flux levels for up to months between 2005-2006. The fact that we have found only one outburst in 98 observations indicates a $\sim 1\%$ duty cycle for outbursts of this kind.

5. Discussion

5.1. P2 as M31*

As in previous studies (Garcia et al. 2005, 2010; Li et al. 2009), our identification of P2 as the X-ray counterpart of M31* rests on positional coincidence. The uncertainty of the registration among the X-ray, optical and radio images is $\sim 0\farcs1\text{-}0\farcs2$, corresponding to a linear size of $\lesssim 1$ pc, and the chance coincidence of an interloping X-ray source is only $\lesssim 1\%$ (Garcia et al. 2010). On the other hand, within 1 pc of the SMBH, members of the eccentric stellar disk (Lauer et al. 1993; Tremaine 1995) almost certainly produce some X-ray emission, which is however difficult to reliably quantify due to the underlying extremely high stellar density. Indeed, the absolute luminosities of the outburst and the subsequent individual detections are only modest ($\lesssim$ a few 10^{37} erg s^{-1}), and by face value, can be attributed to an X-ray binary, e.g., containing an accreting stellar-mass black hole. Most known Galactic black hole binaries show outbursts at a substantial fraction of their L_{Edd}, and in rare cases, some of them also show complex flux variability (e.g., McClintock & Remillard 2006). Hence before addressing the nature of the outburst in the context of M31*, we note that a stellar origin of P2 cannot be completely ruled out.

5.2. Origin of the outburst

The detected outburst adds M31* to a short list of non-active SMBHs that have shown strong X-ray flux variations. Early *ROSAT* observations revealed a handful of X-ray outbursts associated with the nuclei of optically non-active galaxies (cf. Komossa 2002), which are interpreted in terms of tidal disruption of a star passing by the SMBH (Rees 1988). The

absolute luminosities of these outbursts are $\sim 10^{42} - 10^{44}$ erg s^{-1}, a substantial fraction of L_{Edd} of the associated SMBH. Moreover, these outbursts are transient rather than recurrent. These are to be contrasted with the M31* outburst, whose luminosity is $\sim 10^{-8.5}$ L_{Edd} and which is followed by recurrent flux variations, albeit with smaller amplitudes. Hence the M31* outburst is unlikely to be triggered by tidal disruption event.

The outburst is more reminiscent of the strongest X-ray flares seen in Sgr A* (Porquet et al. 2003, 2008). The M31* outburst and Sgr A* flares are similar in strength ($\gtrsim 100$ times relative to the quiescent level), spectral softness and low incidence rate. Hence it is reasonable to speculate that the outburst shares the same physical origin with the Sgr A* flares. In this regard, the individual detections since the outburst are likely flares of smaller amplitudes, again similar to the smaller, but more frequent, flares seen in Sgr A*. However, it appears that the outburst either has triggered or signaled the smaller flares, and the post-outburst mean flux level became more than 10 times the mean flux before the outburst. No such trend has been reported in the long-term X-ray emission from Sgr A*.

At present, the physical origin of the Sgr A* flares remains elusive and most proposed models are phenomenological (e.g., Yuan, Quataert & Narayan 2004; Liu, Melia & Petrosian 2006; Maitra, Markoff & Falcke 2009). In a magnetohydrodynamical model analogous to that developed for the phenomena of coronal mass ejection in our Sun (Lin & Fobes 2000), Yuan et al. (2009a) interpreted the flares as episodic ejection of relativistic plasma blobs ("episodic jets") inflated by magnetic field reconnection in the inner region of the accretion flow. Relativistic particles are accelerated in the reconnection current sheet and are responsible for the X-ray flares. After Sgr A*, M31* is only the second SMBH found to show flaring emission. A comparative study of the two SMBHs should yield important constraints to the flare modeling. Interestingly, M31* and Sgr A* are also the two least active SMBHs known. This refreshes the issue of whether flares are fundamentally related to the lowest accretion rates of LLAGNs, as discussed by Yuan et al. (2004).

Regardless of the exact physical process that produces the active X-ray emission from M31*, it is expected that the average radio emission from M31* has also substantially increased since 2006, by analogy to the associated X-ray/radio flares in Sgr A* (e.g., Marrone et al. 2008). This is also suggested by the so-called fundamental plane of black hole activity (Merloni, Heinz & Di Matteo 2003; see also Yuan et al. 2009b), which empirically relates the X-ray luminosity, radio luminosity and mass of an accreting black hole. We investigated archival VLA observations taken since 2006, but found no useful constraints on the radio variability of M31*, due to poor data quality. New coordinated EVLA observations with much enhanced sensitivities will shed light on the origin of the X-ray flares in M31*. Simultaneous X-ray/radio detection of variability in P2 will help rule out an X-ray binary, whose

radio flux is expected to be well below the sensitivity limit of EVLA.

REFERENCES

Baganoff F.K. et al. 2001, Nature, 413, 45

Bender R., et al. 2005, ApJ, 631, 280

Blandford R.D., Begelman M.C. 1999, MNRAS, 303, L1

Cash W. 1979, ApJ, 228, 939

Crane P.C., Dickel J.R., Cowan J.J. 1992, ApJ, 390, L9

Crane, P.C., Cowan, J.J., Dickel J.R., Roberts D.A. 1993, ApJ, 417, L61

Di Stefano R., et al. 2004, ApJ, 610, 247

Gallo E., Treu T., Marshall P.J., Woo J.-H., Leipski C., Antonucci R. 2010, ApJ, 714, 25

Garcia, M.R., Murray, S.S., Primini, F.A., Forman W.R., McClintock J.E., Christine J. 2000, ApJ, 537, L23

Garcia, M.R., Williams, B.F., Yuan, F., Kong, A.K.H., Primini F.A., Barmby, P., Kaaret, P., Murray, S.S. 2005, ApJ, 632, 1042

Garcia, M.R., et al. 2010, ApJ, 710, 755

Genzel, R., Schödel, R., Ott, T., Eckart, A., Alexander, T., Lacombe, F., Rouan, D., Aschenbach, B. 2003, Nature, 425, 934

Ghez A.M. et al. 2003, ApJ, 586, L127

Ho L.C. 2008, ARA&A, 46, 201

Ho L.C. 2009, ApJ, 699, 626

Komossa S. 2002, Rev. Mod. Astron. 15, 27

Kong A.K.H, Garcia M.R., Primini F.A., Murray S.S., Di Stefano R., McClintock, J.E. 2002, ApJ, 577, 738

Lauer T.R., et al. 1993, AJ, 106, 1436

Li Z., Wang Q.D., Wakker B.P. 2009, MNRAS, 397, 148

Lin J., Forbes T.G. 2000, J. Geophys. Res., 105, 2375

Liu S., Melia F., Petrosian V. 2006, ApJ, 636, 798

Maitra D., Markoff S., Falcke H. 2009, A&A, 508, L13

Marrone D.P. et al. 2008, ApJ, 682, 373

McClintock J.E. & Remillard R.A. 2006, In *Compact Stellar X-ray Sources*, ed. WHG Lewin, M van der Klis, pp. 157 Cambridge: Cambridge Univ.

Merloni A., Heinz S., Di Matteo T. 2003, MNRAS, 345, 1057

Melia F., Falcke H. 2001, ARA&A, 39, 309

Narayan, R., & Yi, I. 1994, ApJ, 428, L13

Porquet D. et al. 2003, A&A, 407, L17

Porquet D. et al. 2008, A&A, 488, 549

Ptak A., Yaqoob T., Mushotzky R., Serlemitsos P., Griffiths R. 1998, ApJ, 501, L37

Quataert E. & Gruzinov A. 2000, ApJ, 539, 809

Rees M.J. 1988, Nature, 333, 523

Tremaine S. 1995, AJ, 110, 628

Weisskopf M.C., Brinkman B., Canizares C., Garmire G., Murray S., Van Speybroeck L.P. 2002, PASP, 114, 1

Yuan F., Quataert E., Narayan R. 2004, ApJ, 606, 894

Yuan F., Lin J., Wu K., Ho L.C., 2009, MNRAS, 395, 2183

Yuan F., Yu Z., Ho L.C., 2009b, ApJ, 703, 1034

Zhang W.M., Soria R., Zhang S.N., Swartz D.A., Liu J.F. 2009, ApJ, 699, 281

Zhao, J.-H., Young, K.H., Herrnstein, R.M., Ho, P.T.P., Tsutsumi, T., Lo, K.Y., Goss, W.M., Bower, G.C. 2003, ApJ, 586, L29
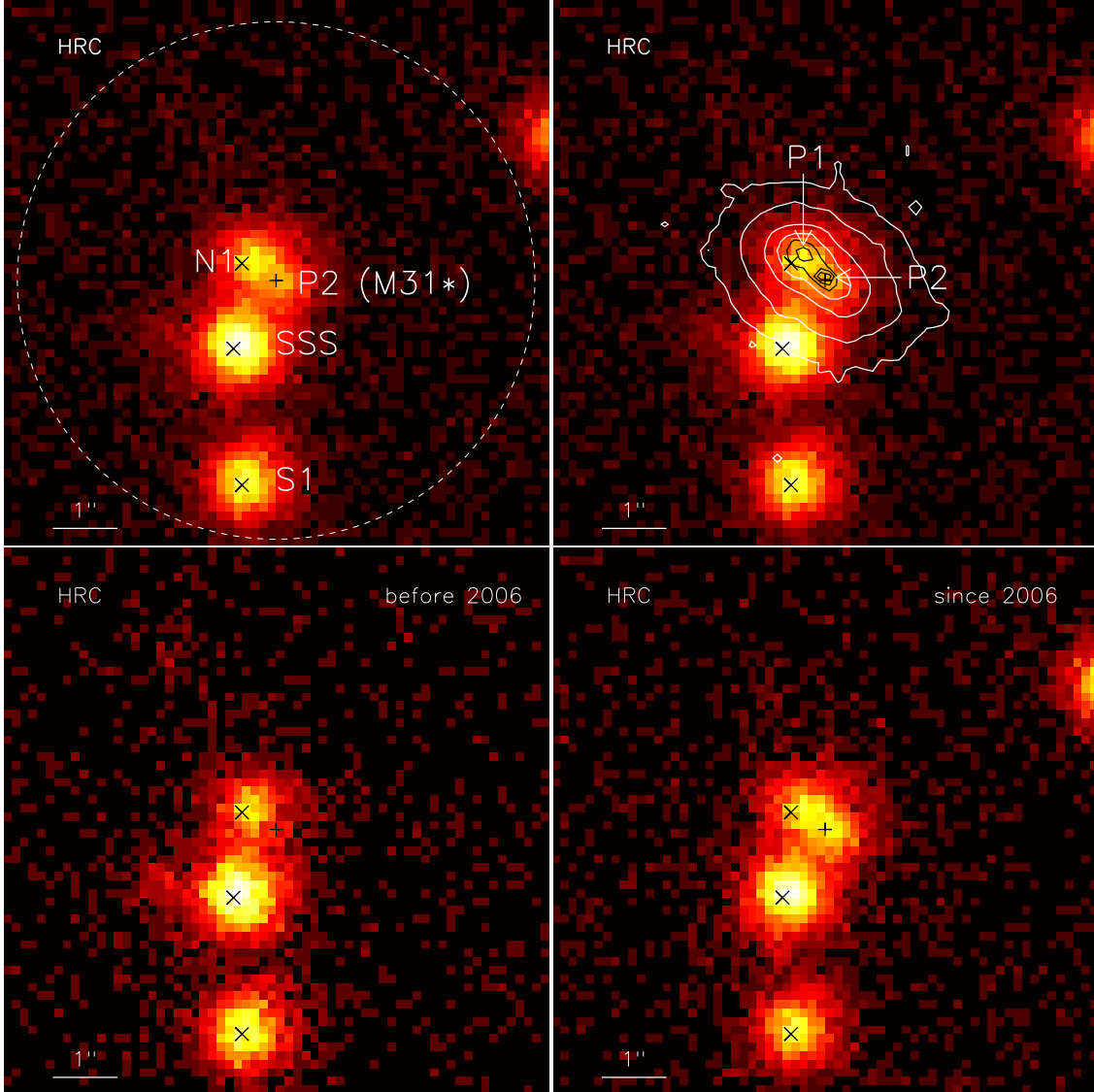
Fig. 1.— *Chandra*/HRC count images of the $8'' \times 8''$ nuclear region of M31, from stacking all observations (*top left* and *top right*), observations taken before 2006 (*bottom left*) and observations taken since 2006 (*bottom right*), respectively. The HRC pixel size is $0.''1318$. The position of M31* is marked by a '+' and labelled as P2. The three extranuclear sources, labelled as, from north to south, N1, SSS and S1, are marked by crosses. The dashed circle encloses the region for fitting. *HST*/ACS F330W intensity contours are plotted in the *top right* panel, highlighting the double nuclei (P1 and P2) in the optical. Note that P2 becomes significantly brighter since 2006.
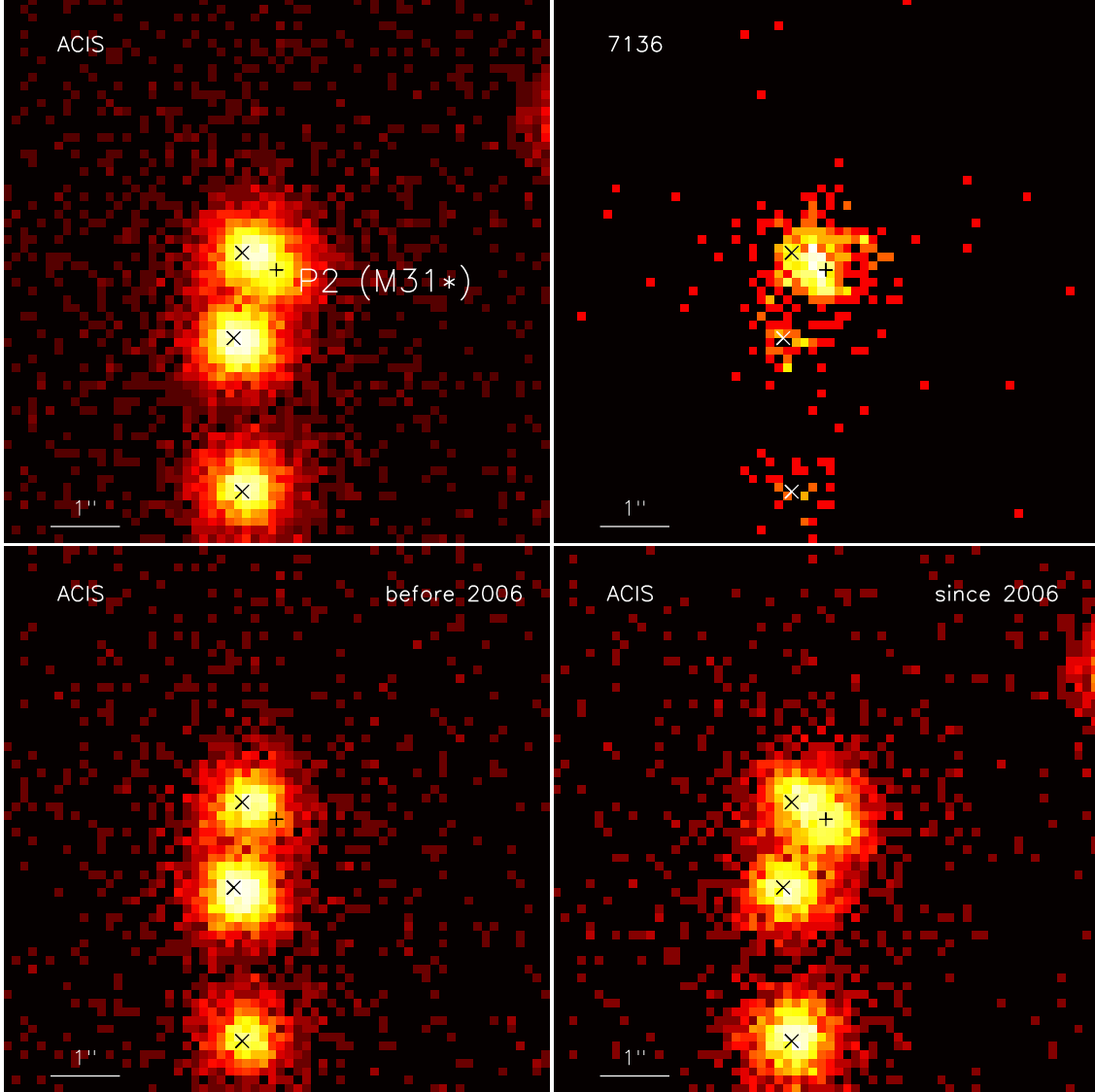
Fig. 2.— *Chandra*/ACIS 0.5-8 keV count images of the 8″×8″ nuclear region of M31, from stacking all observations (*top left*), ObsID 7136 (taken on January 2, 2006) alone (*top right*), stacking observations taken before 2006 (*bottom left*) and stacking observations taken since 2006 except for ObsID 7136 (*bottom right*), respectively. The pixel size is 0″.123, i.e., 1/4 of the ACIS pixel size. The sources are marked in the same way as in Fig. 1. Note the outburst of P2 captured by ObsID 7136.
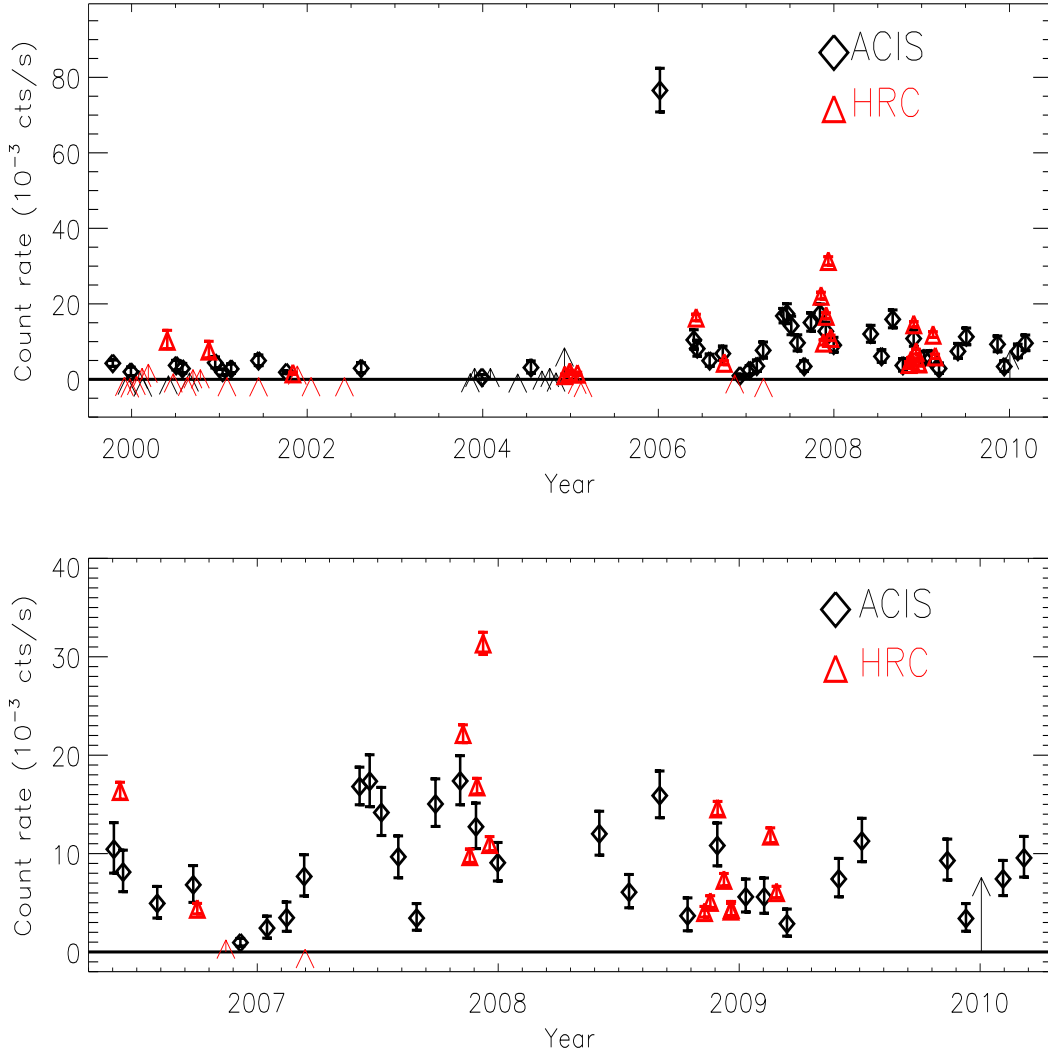
Fig. 3.— *Upper panel*: The decadal X-ray light curve of M31*. An outburst is captured on January 6, 2006, followed by an epoch of frequent flux variation, shown in the *Lower panel*. Arrows represent measurements whose 1σ lower limit is consistent with zero flux. See text for details.